arXiv:1612.02306v1 [cond-mat.str-el] 7 Dec 2016

Maximum entropy analytic continuation for frequency-dependent transport coefficients with non-positive spectral weight

A. Reymbaut[1], A.-M. Gagnon[1], D. Bergeron[1], and A.-M. S. Tremblay[1,2]
[1] *Département de physique and Institut quantique, Université de Sherbrooke, Sherbrooke, Québec, Canada J1K 2R1*
[2] *Canadian Institute for Advanced Research, Toronto, Ontario, Canada, M5G 1Z8*

(Dated: December 8, 2016)

The computation of transport coefficients, even in linear response, is a major challenge for theoretical methods that rely on analytic continuation of correlations functions obtained numerically in Matsubara space. While maximum entropy methods can be used for certain correlation functions, this is not possible in general, important examples being the Seebeck, Hall, Nernst and Reggi-Leduc coefficients. Indeed, positivity of the spectral weight on the positive real-frequency axis is not guaranteed in these cases. The spectral weight can even be complex in the presence of broken time-reversal symmetry. Various workarounds, such as the neglect of vertex corrections or the study of the infinite frequency or Kelvin limits have been proposed. Here, we show that one can define auxiliary response functions that allow to extract the desired real-frequency susceptibilities from maximum entropy methods in the most general multiorbital cases with no particular symmetry. As a benchmark case, we study the longitudinal thermoelectric response and corresponding Onsager coefficient in the single-band two-dimensional Hubbard model treated with dynamical mean-field theory (DMFT) and continuous-time quantum Monte Carlo (CTQMC). We thereby extend to transport coefficients the maximum entropy analytic continuation with auxiliary functions (MaxEntAux method), developed for the study of the superconducting pairing dynamics of correlated materials.

PACS numbers: 71.27.+a, 72.10.-d, 72.10.Bg, 72.15.Jf, 72.20.Pa

a. Introduction. Transport properties are of interest for both fundamental and applied purposes. For example, while thermoelectric power tells us about the nature of charge carriers, materials with large thermoelectric power could lead to various applications, including efficient conversion of heat loss into useful electricity [1–7]. Unfortunately, computing transport coefficients from numerical results is no simple task. Usually, one starts by computing the corresponding response functions in Matsubara frequency using the Kubo formula. For quantum Monte-Carlo data in particular, the most direct way to extract the real-frequency dependent response functions is then to perform maximum entropy analytic continuations (MEACs) [8, 9]. However, as we explain in more details below, MEAC is not always trivial since it requires that the spectral weight of response functions is real and positive, which is not necessarily the case in general.

Many approaches have been investigated to circumvent this major problem for the Seebeck coefficient [10–19], the Hall coefficient [20–24] and the Nernst coefficient [25] for instance, but all of them are either approximations or analytic methods that are exact only in a certain frequency limit. The most common approach consists in neglecting vertex corrections, in which case it is possible to compute transport coefficients directly from the single-particle spectral weight. This is not possible when vertex corrections are included, which seems to be a necessary step in understanding the record-breaking thermopower of FeSe [3] for instance. In that case, a more versatile approach, that would extend to all transport quantities, still remains to be developed. This is the problem that we address here by generalizing the MaxEntAux method developed for fermionic response functions [26, 27] to the case of bosonic response functions with non-positive spectral weights [28]. We first describe this method for the most general multiorbital system with no particular symmetry before presenting a benchmark case for the uniform longitudinal thermoelectric response (or uniform Seebeck response) of a single-band two-dimensional Hubbard model treated with dynamical mean-field theory (DMFT) [29] and continuous-time quantum Monte Carlo (CTQMC) [30]. The DC limit is also compared to a low-temperature approximation [31], detailed in the supplemental material Ref. [32]. Some of the issues associated with convergence of Matsubara frequency sums are also discussed there [32].

b. Bosonic response functions without positive spectral weight Let us define the correlation function between general bosonic operators $\hat{\mathcal{O}}_{\vec{k}\gamma}$ and $\hat{\mathcal{O}}_{\vec{k}\delta}$ by

$$\chi_{\gamma\delta}(\vec{k},\tau) = -\left\langle \hat{\mathcal{T}}_\tau\, \hat{\mathcal{O}}_{\vec{k}\gamma}(\tau)\, \hat{\mathcal{O}}^\dagger_{\vec{k}\delta}(0)\right\rangle_{\hat{\mathcal{H}}}, \qquad (1)$$

where $\vec{k}$ is wave vector, the average is taken with respect to the grand-canonical ensemble for Hamiltonian $\hat{\mathcal{H}}$ (with eigenvectors $|m\rangle$ and eigenenergies H_m) and $\hat{\mathcal{T}}_\tau$ is the bosonic imaginary-time ordering operator. In the case of current operators, that we consider in this paper, γ and δ stand for the electrical (E) or thermal (T) nature of the current operators and also for spatial direction (x, y or z), band, and spin indices. The discrete Fourier transform to bosonic Matsubara frequency space, $\chi_{\gamma\delta}(\vec{k}, i\omega_n) = \int_0^\beta \mathrm{d}\tau\, e^{i\omega_n\tau}\chi_{\gamma\delta}(\vec{k},\tau)$, is related to the spec-

tral weight $\chi''_{\gamma\delta}(\vec{k},\omega)$ through the relation

$$\chi_{\gamma\delta}(\vec{k},i\omega_n) = \int_0^\beta \mathrm{d}\tau\, e^{i\omega_n\tau}\chi_{\gamma\delta}(\vec{k},\tau) = \int \frac{\mathrm{d}\omega}{\pi}\,\frac{\chi''_{\gamma\delta}(\vec{k},\omega)}{\omega - i\omega_n}\,. \tag{2}$$

This spectral weight is essential, for example, to obtain the finite-frequency behavior of the Hall conductivity (related to the Faraday effect) that obeys the analog of a f-sum rule [33, 34].

The non-triviality of the MEAC for a general response function arises because this method requires that

$$\forall\omega,\ \omega\,\chi''_{\gamma\delta}(\vec{k},\omega) \geq 0 \quad \text{and} \quad \chi''_{\gamma\delta}(\vec{k},\omega) \in \mathbb{R} \tag{3}$$

for bosonic data. However, the Lehmann representation

$$\frac{\pi}{\mathcal{Z}}\sum_{mm'} e^{-\beta H_m}\left[e^{\beta\omega}-1\right]\langle m|\hat{\mathcal{O}}_{\vec{k}\gamma}|m'\rangle\langle m'|\hat{\mathcal{O}}^\dagger_{\vec{k}\delta}|m\rangle \times\delta(\omega-(H_m-H_{m'})) \tag{4}$$

for $\chi''_{\gamma\delta}(\vec{k},\omega)$, where $\mathcal{Z}$ is the partition function of the system, tells us that while this condition is obviously satisfied if $\delta\equiv\gamma$ since

$$\langle m|\hat{\mathcal{O}}_{\vec{k}\gamma}|m'\rangle\langle m'|\hat{\mathcal{O}}^\dagger_{\vec{k}\gamma}|m\rangle = |\langle m|\hat{\mathcal{O}}_{\vec{k}\gamma}|m'\rangle|^2 \geq 0\,, \tag{5}$$

this special case corresponds only to purely electric or purely thermal longitudinal responses, hence transverse response functions in the presence of a symmetry-breaking magnetic field or even, more simply, the thermoelectric response, cannot be obtained with the standard approach.

c. MaxEntAux Method for the General Case. Consider the general correlation function Eq. (1). Generalizing the approach of Ref. [26], we define the mixed operator

$$\hat{\mathcal{A}}_{\vec{k}\gamma\delta,\lambda} = \hat{\mathcal{O}}_{\vec{k}\gamma} + \lambda\,\hat{\mathcal{O}}^\dagger_{-\vec{k}\delta}\,. \tag{6}$$

With the usual Matsubara imaginary-time evolution $\hat{\mathcal{O}}_{\vec{k}\gamma}(\tau) = e^{H\tau}\hat{\mathcal{O}}_{\vec{k}\gamma}e^{-H\tau}$ and $\hat{\mathcal{O}}^\dagger_{\vec{k}\gamma}(\tau) = e^{H\tau}\hat{\mathcal{O}}^\dagger_{\vec{k}\gamma}e^{-H\tau}$ we define the auxiliary susceptibility

$$\chi^{aux\,1}_{\gamma\delta,\lambda}(\vec{k},\tau) = -\left\langle \hat{\mathcal{T}}_\tau\,\hat{\mathcal{A}}_{\vec{k}\gamma\delta,\lambda}(\tau)\,\hat{\mathcal{A}}^\dagger_{\vec{k}\gamma\delta,\lambda}(0)\right\rangle_{\hat{\mathcal{H}}}\,, \tag{7}$$

where λ is an arbitrary real constant that, in principle, ensures conversion of units between two possibly different current operators in $\hat{\mathcal{A}}_{\vec{k}\gamma\delta,\lambda}$. The Lehmann representation allows one to check that the auxiliary susceptibility Eq. (7) satisfies the condition Eq. (3) and can thus be analytically continued using standard maximum entropy methods. With hermitian operators, we have $\hat{\mathcal{O}}^\dagger_{-\vec{k}\gamma} = \hat{\mathcal{O}}_{\vec{k}\gamma}$ so that one finds

$$\chi^{aux\,1}_{\gamma\delta,\lambda}(\vec{k},\tau) = \chi_{\gamma\gamma}(\vec{k},\tau) + \lambda^2\chi_{\delta\delta}(\vec{k},\tau) + \lambda\,\chi_{\gamma\delta}(\vec{k},\tau) + \lambda\left[\chi_{\gamma\delta}(\vec{k},\tau)\right]^*. \tag{8}$$

Using the spectral representation Eq. (2) for the susceptibility, Eq. (8) can then be obtained in Matsubara frequencies:

$$\begin{aligned}\chi^{aux\,1}_{\gamma\delta,\lambda}(\vec{k},i\omega_n) &= \chi_{\gamma\gamma}(\vec{k},i\omega_n) + \lambda^2\chi_{\delta\delta}(\vec{k},i\omega_n) + \lambda\,\chi_{\gamma\delta}(\vec{k},i\omega_n) + \lambda\left[\chi_{\gamma\delta}(\vec{k},-i\omega_n)\right]^* &(9)\\ &= \chi_{\gamma\gamma}(\vec{k},i\omega_n) + \lambda^2\chi_{\delta\delta}(\vec{k},i\omega_n) + \lambda\int\frac{\mathrm{d}\omega}{\pi}\,\frac{\chi''_{\gamma\delta}(\vec{k},\omega)+\chi''^*_{\gamma\delta}(\vec{k},\omega)}{\omega-i\omega_n}\,. &(10)\end{aligned}$$

To find the missing information, we define, by analogy with Eq. (6), a second mixed operator

$$\hat{\mathcal{B}}_{\vec{k}\gamma\delta,\lambda} = \hat{\mathcal{O}}_{\vec{k}\gamma} + i\lambda\,\hat{\mathcal{O}}^\dagger_{-\vec{k}\delta}\,, \tag{11}$$

and a corresponding second auxiliary susceptibility satisfying the condition Eq. (3)

$$\chi^{aux\,2}_{\gamma\delta,\lambda}(\vec{k},\tau) = -\left\langle \hat{\mathcal{T}}_\tau\,\hat{\mathcal{B}}_{\vec{k}\gamma\delta,\lambda}(\tau)\,\hat{\mathcal{B}}^\dagger_{\vec{k}\gamma\delta,\lambda}(0)\right\rangle_{\hat{\mathcal{H}}}\,. \tag{12}$$

We could have chosen another constant λ' instead of λ. We keep λ for simplicity. Then, by analogy with Eq. (10), we find

$$\chi^{aux\,2}_{\gamma\delta,\lambda}(\vec{k},i\omega_n) = \chi_{\gamma\gamma}(\vec{k},i\omega_n) + \lambda^2\chi_{\delta\delta}(\vec{k},i\omega_n) - i\lambda\int\frac{\mathrm{d}\omega}{\pi}\,\frac{\chi''_{\gamma\delta}(\vec{k},\omega)-\chi''^*_{\gamma\delta}(\vec{k},\omega)}{\omega-i\omega_n} \tag{13}$$

The MEAC of the two auxiliary susceptibilities gives the corresponding real spectral weights satisfying the condition Eq. (3), which are formally given by

$$\chi''^{\,aux\,1}_{\gamma\delta,\lambda}(\vec{k},\omega) = \chi''_{\gamma\gamma}(\vec{k},\omega) + \lambda^2\chi''_{\delta\delta}(\vec{k},\omega) + \lambda\left[\chi''_{\gamma\delta}(\vec{k},\omega) + \chi''^*_{\gamma\delta}(\vec{k},\omega)\right]\,, \tag{14}$$

$$\chi''^{\,aux\,2}_{\gamma\delta,\lambda}(\vec{k},\omega) = \chi''_{\gamma\gamma}(\vec{k},\omega) + \lambda^2\chi''_{\delta\delta}(\vec{k},\omega) - i\lambda\left[\chi''_{\gamma\delta}(\vec{k},\omega) - \chi''^*_{\gamma\delta}(\vec{k},\omega)\right]\,. \tag{15}$$

The spectral weights of the form $\chi''_{\gamma\gamma}(\vec{k},\omega)$ also satisfy the condition Eq. (3). From the above, one can easily extract

the needed complex-valued spectral weight $\chi''_{\gamma\delta}(\vec{k},\omega)$ via

$$\chi''_{\gamma\delta}(\vec{k},\omega) = \frac{1}{2\lambda}\left\{\chi''^{\,aux\,1}_{\gamma\delta,\lambda}(\vec{k},\omega) + i\,\chi''^{\,aux\,2}_{\gamma\delta,\lambda}(\vec{k},\omega) - (1+i)[\chi''_{\gamma\gamma}(\vec{k},\omega) + \lambda^2\chi''_{\delta\delta}(\vec{k},\omega)]\right\} . \tag{16}$$

In the case of current operators, this is valid for any kind of response function in the multi-orbital case, with or without inversion or time-reversal symmetry.

d. Practical Example for the Uniform Seebeck Response. The study of uniform longitudinal thermoelectricity relies only on the three response functions for electrical and thermal currents $\chi_{E_xE_x}$, $\chi_{E_xT_x}$ and $\chi_{T_xT_x}$, more generally defined as:

$$\chi_{\gamma\delta}(\tau) = -\left\langle \hat{\mathcal{T}}_\tau\, \hat{\jmath}_\gamma(\tau)\, \hat{\jmath}_\delta(0)\right\rangle_{\hat{\mathcal{H}}} , \tag{17}$$

where we explicitly wrote the current operators $\hat{\jmath}_\gamma$, standing for the electrical and thermal currents at $\vec{k}=\vec{0}$ (with $\hat{\jmath}^\dagger_{\vec{k}\gamma} = \hat{\jmath}_{-\vec{k}\gamma}$ in general). As mentioned above, while $\chi_{E_xE_x}$ and $\chi_{T_xT_x}$ can be analytically continued through standard maximum entropy methods, $\chi_{E_xT_x}$ cannot be. For this practical example, we focus on a system with time-reversal symmetry. In that case, one can show that any spectral weight $\chi''_{\gamma\delta}(\omega)$ is real and odd in real frequency when the two operators involved have the same signature under time-reversal. The spectral representation Eq. (2) then implies that $\chi_{\gamma\delta}(i\omega_n)$ is real and even in Matsubara frequency, thus reducing Eq. (9) to

$$\chi^{aux}_\lambda(i\omega_n) = \chi_{E_xE_x}(i\omega_n) + \lambda^2\chi_{T_xT_x}(i\omega_n) + 2\lambda\,\chi_{E_xT_x}(i\omega_n) . \tag{18}$$

Defining the frequency-dependent Onsager coefficients through

$$\mathrm{Re}\,\mathcal{L}_{\gamma\delta}(\omega) = \lim_{\vec{k}\to\vec{0}}\left[\frac{\chi''_{\gamma\delta}(\vec{k},\omega)}{\omega}\right] . \tag{19}$$

the bosonic Matsubara frequency result Eq. (18) immediately translates to

$$\mathcal{L}_{E_xT_x}(\omega) = \frac{1}{2\lambda}\left[\mathcal{L}^{aux}_\lambda(\omega) - \mathcal{L}_{E_xE_x}(\omega) - \lambda^2\mathcal{L}_{T_xT_x}(\omega)\right] . \tag{20}$$

e. Model and method We consider the two-dimensional square lattice described by the single-band Hubbard model

$$\hat{\mathcal{H}} = -t\sum_{\langle i,j\rangle\,\sigma}\left(\hat{c}^\dagger_{i\sigma}\,\hat{c}_{j\sigma} + h.c\right) + U\sum_i \hat{n}_{i\uparrow}\,\hat{n}_{i\downarrow} - \mu\sum_i \hat{n}_i , \tag{21}$$

with t the nearest-neighbor hopping, U the on-site Coulomb repulsion and μ the chemical potential. We take $t\equiv 1$ as our energy unit and otherwise work in natural units ($\hbar\equiv 1$ and $k_B\equiv 1$).

When vertex corrections are included, the direct MEAC of $\chi_{\gamma\delta}(i\omega_n)$ is mandatory. But to benchmark our approach, we consider a case where vertex corrections are neglected so that the transport coefficients can be computed directly from the single particle spectral weight using

$$\chi''_\nu(\omega) = \pi T\sum_\sigma\int_{-4t}^{4t} \mathrm{d}\varepsilon \int \mathrm{d}\omega'\,\mathcal{T}(\varepsilon)\,\mathcal{A}(\varepsilon,\omega')\,\mathcal{A}(\varepsilon,\omega'+\omega) \times [f(\omega') - f(\omega'+\omega)]\left(\omega' + \frac{\omega}{2}\right)^\nu , \tag{22}$$

where f is the Fermi-Dirac distribution and $\mathcal{A}(\vec{k},\omega)$ is the spectral function containing the non-interacting square-lattice dispersion $\varepsilon_{\vec{k}}$ and normalized so that $\int \mathrm{d}\omega\,\mathcal{A}(\vec{k},\omega) = 1$. In this notation, $\chi''_{\nu=0}(\omega) = \chi''_{E_xE_x}(\omega)$, $\chi''_{\nu=1}(\omega) = \chi''_{E_xT_x}(\omega)$, and $\chi''_{\nu=2}(\omega) = \chi''_{T_xT_x}(\omega)$ [19]. Here, the usual integral over wave-vectors has been replaced by an integral over the band energies ε weighted by the longitudinal transport function [35]

$$\mathcal{T}(\varepsilon) = \sum_{\vec{k}}\left(\frac{\partial\varepsilon_{\vec{k}}}{\partial k_x}\right)^2 \delta(\varepsilon - \varepsilon_{\vec{k}}) = -\frac{1}{2}\int_{-4t}^{\varepsilon} z N_0(z)\,\mathrm{d}z \tag{23}$$

containing the non-interacting density of states N_0, normalized so that $\int N_0(z)\,\mathrm{d}z = 1$.

Our test is performed as follows. Given the value of $\chi''_\nu(\omega)$ in Eq. (22), we obtain Matsubara susceptibilities $\chi_\nu(i\omega_n)$ from the spectral representation Eq. (2). We then add a Gaussian noise with a relative error of 10^{-3} on each Matsubara frequency in order to mimic quantum Monte-Carlo statistical error. Finally, we use the maximum entropy code OmegaMaxEnt [36] to extract the analytically continued spectral weights $\chi''_\nu(\omega)$, that can then be compared with the starting values. While $\chi_{E_xE_x}(i\omega_n)$ and $\chi_{T_xT_x}(i\omega_n)$ are analytically continued directly, the MaxEntAux formula Eq. (18) is used to analytically continue $\chi_{E_xT_x}(i\omega_n)$.

Any physical single-particle spectral weight $\mathcal{A}(\vec{k},\omega)$ could have been used for the test, but to be as realistic as possible, we used one obtained from an actual calculation. We take $U=14$, temperature $T=1$, and set the chemical potential so that filling is $n=0.85$, a case studied in Ref. [19]. It is at high-temperature that analytic continuation is most difficult and that the sign change in the frequency-dependent thermoelectric spectral weight is largest [19]. A more thorough comparison and results at a lower temperature $T=1/10$ are presented in the supplemental material Ref. [32]. We use dynamical mean-field theory (DMFT) [29] solved with continuous-time quantum Monte Carlo (CTQMC) [30] to simulate our system and compute the local fermionic Matsubara-frequency self-energy $\Sigma(ip_n)$ which is analytically continued to give us our starting $\mathcal{A}(\vec{k},\omega)$ and corresponding $\chi''_\nu(\omega)$.

f. Results. Fig. 1 compares the initial real-frequency Onsager coefficients $\mathcal{L}_{\gamma\delta}(\omega)$ obtained from $\chi''_\nu(\omega)$ Eqs. (19) and (22) to those obtained after MEACs of the Matsubara data with the MaxEntAux method Eq. (20) with $\lambda = 0.3$. The comparison shows a good agreement for all cases. In particular, the real part of $\mathcal{L}_{E_xT_x}(\omega)$ has a large region of negative spectral weight that is remarkably well reproduced by our approach. The imaginary part of $\mathcal{L}_{E_xT_x}(\omega)$ is obtained from Kramers-Kronig. MEACs oscillate slightly around the initial data (dashed lines). The same comparison, presented for different values of λ in the supplemental material Ref. [32], demonstrates the robustness of the MaxEntAux method with varying λ.

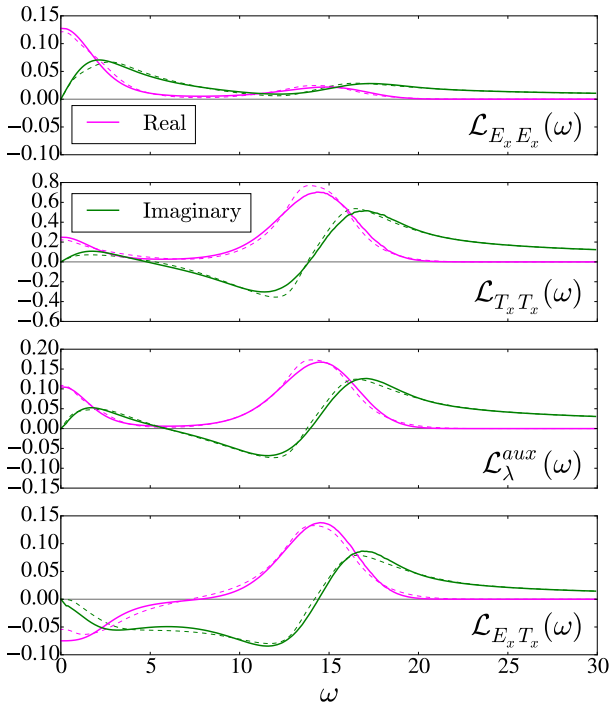

Figure 1. Comparison for $T = 1$, $U = 14$ between the initial real-frequency Onsager coefficients Eq. (19) calculated with Eq. (22) (dashed lines) to those obtained after analytic continuation of the Matsubara data with an added relative noise of 10^{-3} (solid lines) using the MaxEntAux method with $\lambda = 0.3$.

Fig. 2 shows the electrical conductivity σ, the Seebeck coefficient S and the thermal conductivity κ, defined by

$$\sigma = \frac{e^2}{T}\,\mathcal{L}_{E_xE_x}\,, \tag{24}$$

$$S = -\frac{1}{eT}\,\frac{\mathcal{L}_{E_xT_x}}{\mathcal{L}_{E_xE_x}}\,, \tag{25}$$

$$\kappa = \frac{1}{T^2}\left[\mathcal{L}_{T_xT_x} - \frac{\mathcal{L}^2_{E_xT_x}}{\mathcal{L}_{E_xE_x}}\right], \tag{26}$$

where the convention [19, 37] chosen for the Onsager coefficients $\mathcal{L}_{\gamma\delta} = \lim_{\omega\to 0}\mathcal{L}_{\gamma\delta}(\omega)$ is presented in the supplemental material Ref. [32]. Here, we take the electrical charge $e \equiv 1$, so that the experimental value of the Seebeck coefficient is retrieved by multiplying our value by $k_B/e = 86.3\ \mu\text{V.K}^{-1}$.

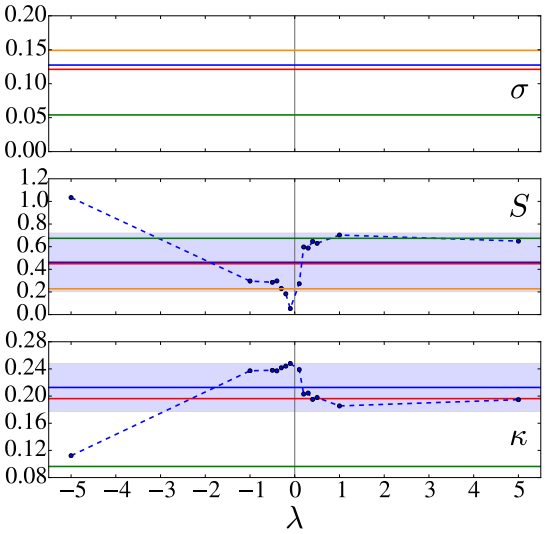

Figure 2. Electrical conductivity, Seebeck coefficient, and thermal conductivity for $T = 1, U = 14$ from Eqs. (24), (25), and (26) respectively. Comparison between the benchmark values (red solid lines) and those of the MaxEntAux method applied to the Matsubara frequency results with an added relative noise of 10^{-3} (blue dashed lines). The blue solid lines and blue area represent the mean value and the error span of the λ-dependent results (blue points), respectively. The orange lines show the results of Ref. [19] and the green lines those for the low-temperature approximation Eq. (27).

Transport quantities obtained from the initial spectral weight Eq. (22) are compared in Fig. 2 to those obtained from the MaxEntAux method. The relative error on the electrical conductivity remains under 10%. Although with perfect analytic continuation the λ-dependence of $\mathcal{L}_{E_xT_x}$ in Eq. (20) would drop out, in practice it does not, so that S and κ are λ-dependent. To obtain a more significant estimate for S and κ, we compute the averages over λ. Comparing them with the initial quantities, we find that the relative error is under 10%. Comparison with the results of Ref. [19] and with the low-temperature approximation [31, 38] $\mathcal{L}_{\gamma\delta} \simeq (\beta/\pi)^2\,\mathcal{L}_{\gamma\delta}(\tau = \beta/2)$ or

$$\mathcal{L}_{\gamma\delta} \simeq \frac{\beta^2}{\pi^2}\int_{-\infty}^{+\infty} \mathrm{d}\omega\, \frac{\chi''_{\gamma\delta}(\vec{0},\omega)}{2\sinh\left(\frac{\beta\omega}{2}\right)} \tag{27}$$

shows that, for the case studied here, the MaxEntAux method gives more accurate values than Refs. [31, 38] for all transport coefficients [39]. The supplemental material Ref. [32] discusses lower temperatures.

g. Conclusion. The above results open the way to the systematic exploration of transport properties obtained from numerical calculations in Matsubara space in any system, with or without vertex corrections. While

benchmarks were shown for the uniform Seebeck response $\chi''_{E_xT_x}(\omega)$, even less trivial problems can be investigated. For instance, the Hall $\chi''_{E_xE_y}(\vec{k},\omega)$ and Nernst $\chi''_{E_xT_y}(\vec{k},\omega)$ response functions are of interest in cases where time-reversal symmetry is broken by a magnetic field.

h. Acknowledgments. We are indebted to S. Verret, D. Sénéchal, J. Gukelberger, R. Nourafkan and B. S. Shastry for fruitful discussions. This work has been supported by the Natural Sciences and Engineering Research Council of Canada (NSERC) under grant RGPIN-2014-04584, and by the Research Chair in the Theory of Quantum Materials (A.-M.S. T.). Simulations were performed on computers provided by Canadian Foundation for Innovation, the Ministère de l'Éducation des Loisirs et du Sport (Québec), Calcul Québec, and Compute Canada.

[1] I. Terasaki, Y. Sasago, and K. Uchinokura, "Large thermoelectric power in naco$_2$o$_4$ single crystals," Phys. Rev. B **56**, R12685–R12687 (1997).
[2] A. Bentien, S. Johnsen, G. K. H. Madsen, B. B. Iversen, and F. Steglich, "Colossal seebeck coefficient in strongly correlated semiconductor fesb 2," EPL (Europhysics Letters) **80**, 17008 (2007).
[3] Jan M. Tomczak, K. Haule, T. Miyake, A. Georges, and G. Kotliar, "Thermopower of correlated semiconductors: Application to feas$_2$ and fesb$_2$," Phys. Rev. B **82**, 085104 (2010).
[4] P. Sun, M. Søndergaard, B.B. Iversen, and F. Steglich, "Strong electron correlations in fesb2," Annalen der Physik **523**, 612–620 (2011).
[5] Louis-François Arsenault, B. Sriram Shastry, Patrick Sémon, and A.-M. S. Tremblay, "Entropy, frustration, and large thermopower of doped mott insulators on the fcc lattice," Phys. Rev. B **87**, 035126 (2013).
[6] A. Ozaeta, P. Virtanen, F. S. Bergeret, and T. T. Heikkilä, "Predicted very large thermoelectric effect in ferromagnet-superconductor junctions in the presence of a spin-splitting magnetic field," Phys. Rev. Lett. **112**, 057001 (2014).
[7] S. Kolenda, M. J. Wolf, and D. Beckmann, "Observation of thermoelectric currents in high-field superconductor-ferromagnet tunnel junctions," Phys. Rev. Lett. **116**, 097001 (2016).
[8] Mark Jarrell and J. E. Gubernatis, "Bayesian inference and the analytic continuation of imaginary-time quantum Monte Carlo data," Physics Reports **269**, 133–195 (1996).
[9] Anders W. Sandvik, "Stochastic method for analytic continuation of quantum monte carlo data," Phys. Rev. B **57**, 10287–10290 (1998).
[10] Gerardo Beni, "Thermoelectric power of the narrow-band hubbard chain at arbitrary electron density: Atomic limit," Phys. Rev. B **10**, 2186–2189 (1974).
[11] P. M. Chaikin and G. Beni, "Thermopower in the correlated hopping regime," Phys. Rev. B **13**, 647–651 (1976).
[12] Gunnar Pálsson and Gabriel Kotliar, "Thermoelectric response near the density driven mott transition," Phys. Rev. Lett. **80**, 4775–4778 (1998).
[13] W. Koshibae, K. Tsutsui, and S. Maekawa, "Thermopower in cobalt oxides," Phys. Rev. B **62**, 6869–6872 (2000).
[14] V. S. Oudovenko and G. Kotliar, "Thermoelectric properties of the degenerate hubbard model," Phys. Rev. B **65**, 075102 (2002).
[15] Hiroshi Kontani, "General formula for the thermoelectric transport phenomena based on fermi liquid theory: Thermoelectric power, nernst coefficient, and thermal conductivity," Phys. Rev. B **67**, 014408 (2003).
[16] B. Sriram Shastry, "Sum rule for thermal conductivity and dynamical thermal transport coefficients in condensed matter," Phys. Rev. B **73**, 085117 (2006).
[17] B. Sriram Shastry, "Electrothermal transport coefficients at finite frequencies," Reports on Progress in Physics **72**, 016501 (2009).
[18] Shiladitya Chakraborty, Dimitrios Galanakis, and Philip Phillips, "Emergence of particle-hole symmetry near optimal doping in high-temperature copper oxide superconductors," Phys. Rev. B **82**, 214503 (2010).
[19] Wenhu Xu, Cédric Weber, and Gabriel Kotliar, "High-frequency thermoelectric response in correlated electronic systems," Phys. Rev. B **84**, 035114 (2011).
[20] B. Sriram Shastry, Boris I. Shraiman, and Rajiv R. P. Singh, "Faraday rotation and the hall constant in strongly correlated fermi systems," Phys. Rev. Lett. **70**, 2004–2007 (1993).
[21] F. F. Assaad and M. Imada, "Hall coefficient for the two-dimensional hubbard model," Phys. Rev. Lett. **74**, 3868–3871 (1995).
[22] Brijesh Kumar and B. S. Shastry, "Superconductivity in coo$_2$ layers and the resonating valence bond mean-field theory of the triangular lattice $t-j$ model," Phys. Rev. B **68**, 104508 (2003).
[23] Brijesh Kumar and B. S. Shastry, "Erratum: Superconductivity in coo$_2$ layers and the resonating valence bond mean-field theory of the triangular lattice $t-j$ model [phys. rev. b 68, 104508 (2003)]," Phys. Rev. B **69**, 059901 (2004).
[24] Jan O. Haerter and B. Sriram Shastry, "Hall number, optical sum rule and carrier density for the t-t'-j model," Phys. Rev. B **77**, 045127 (2008).
[25] Wenhu Xu, Kristjan Haule, and Gabriel Kotliar, "Hidden fermi liquid, scattering rate saturation, and nernst effect: A dynamical mean-field theory perspective," Phys. Rev. Lett. **111**, 036401 (2013).
[26] A. Reymbaut, D. Bergeron, and A.-M. S. Tremblay, "Maximum entropy analytic continuation for spectral functions with nonpositive spectral weight," Phys. Rev. B **92**, 060509(R) (2015).
[27] A. Reymbaut, M. Charlebois, M. Fellous Asiani, L. Fratino, P. Sémon, G. Sordi, and A.-M. S. Tremblay, "Antagonistic effects of nearest-neighbor repulsion on the superconducting pairing dynamics in the doped mott insulator regime," Phys. Rev. B **94**, 155146 (2016).
[28] A.-M. Gagnon, *Une méthode alternative pour obtenir le pouvoir thermoélectrique à température finie*, M.sc., Uni-

versité de Sherbrooke (2016).
[29] A. Georges, G. Kotliar, W. Krauth, and M. J. Rozenberg, "Dynamical mean-field theory of strongly correlated fermion systems and the limit of infinite dimensions," Rev. Mod. Phys. **68**, 13–25 (1996).
[30] Emanuel Gull, Andrew J. Millis, Alexander I. Lichtenstein, Alexey N. Rubtsov, Matthias Troyer, and Philipp Werner, "Continuous-time Monte Carlo methods for quantum impurity models," Rev. Mod. Phys. **83**, 349–404 (2011).
[31] Mohit Randeria, Nandini Trivedi, Adriana Moreo, and Richard T. Scalettar, "Pairing and spin gap in the normal state of short coherence length superconductors," Phys. Rev. Lett. **69**, 2001–2004 (1992).
[32] See appendices for the choice of convention for the Onsager coefficients (identical to that of Ref. [37]). Explanations behind the low-temperature approximation Eq. (27) [31] are given. We also present results at $U = 14$, $T = 1/10$ and $T = 1$ including the response functions' spectral weights along with a more thorough comparison with Ref. [19] and the approximation Eq. (27). It is also shown how the results are affected by the choice of λ in Eqs. (6) and (11). We end with new expressions [28] for the bubble part of the uniform susceptibilities that are convergent upon summation over internal Matsubara frequencies [40]. The convergence of the corresponding expressions given in Ref. [41] is discussed. In addition, we include examples of data files used for obtaining the first figure of this paper with OmegaMaxEnt [36].
[33] S. Spielman, Beth Parks, J. Orenstein, D. T. Nemeth, Frank Ludwig, John Clarke, Paul Merchant, and D. J. Lew, "Observation of the quasiparticle hall effect in superconducting $Yba_2cu_3o_{7-\delta}$," Phys. Rev. Lett. **73**, 1537–1540 (1994).
[34] H. D. Drew and P. Coleman, "Sum rule for the optical hall angle," Phys. Rev. Lett. **78**, 1572–1575 (1997).
[35] Louis-François Arsenault and A.-M. S. Tremblay, "Transport functions for hypercubic and bethe lattices," Phys. Rev. B **88**, 205109 (2013).
[36] Dominic Bergeron and A.-M. S. Tremblay, "Algorithms for optimized maximum entropy and diagnostic tools for analytic continuation," Phys. Rev. E **94**, 023303 (2016).
[37] G. D. Mahan, *Many-Particle Physics* (Kluwer Academic - Plenum publishers, New-York, 2000).
[38] X. Chen, J. P. F. LeBlanc, and E. Gull, "Knight shifts, nuclear spin-relaxation rates, and spin echo decay times in the pseudogap regime of the cuprates: Simulation and relation to experiment," ArXiv e-prints (2016), arXiv:1607.05655 [cond-mat.str-el].
[39] Notice that this approximation is not valid in the renormalized classical regime since the convergence of the integral in Eq. (27) is controlled by the susceptibility instead of the sinh factor in this regime.
[40] Dominic Bergeron, Vasyl Hankevych, Bumsoo Kyung, and A.-M. S. Tremblay, "Optical and dc conductivity of the two-dimensional hubbard model in the pseudogap regime and across the antiferromagnetic quantum critical point including vertex corrections," Phys. Rev. B **84**, 085128 (2011).
[41] Indranil Paul and Gabriel Kotliar, "Thermal transport for many-body tight-binding models," Phys. Rev. B **67**, 115131 (2003).

Appendix A: Summary of supplemental material

In Sec. B, we detail the choice of convention for the Onsager coefficients, identical to the one in Ref. [37]. In Sec. C, we explain the low-temperature approximation taken from Ref. [31]. We recapitulate our procedure for benchmarks and present in Sec. D additional results at $T = 1/10$ and $T = 1$ for the spectral weights of relevant susceptibilities. We continue with more benchmark tests on the Onsager coefficients and a more thorough comparison with the low-temperature approximation from Ref. [31] in Sec. E. Combinations of Onsager coefficients are related to the transport coefficients. We benchmark those in Sec. F. Finally, in Sec. G, we give new expressions, taken from Ref. [28], for the bubble part of the uniform susceptibilities that are convergent upon summation over internal Matsubara frequencies. The convergence of the corresponding expressions given in Ref. [41] is discussed. Note that the independence of the results on the value of λ is discussed in Sec. D and Sec. E.

In this supplemental material, we do not consider the case where a magnetic field is applied. In other words, time-reversal invariance is assumed.

Appendix B: Convention for the Onsager Coefficients.

The relationship between the Onsager coefficients

$$\mathcal{L}_{\gamma\delta} = \lim_{\omega\to 0} \mathrm{Re}\,\mathcal{L}_{\gamma\delta}(\omega) = \lim_{\omega\to 0}\lim_{\vec{k}\to\vec{0}} \left[\frac{\chi''_{\gamma\delta}(\vec{k},\omega)}{\omega}\right] \tag{B1}$$

and the relevant transport quantities always depends on the choice made for the form of the phenomenological equations describing how electrical and heat currents are induced by gradients of electrical potential and temperature in the uniform and static limits. For instance, in the case of the longitudinal thermoelectric response (or Seebeck response), we chose the same equations as Ref. [37]:

$$\vec{j}_{E_x} = \mathcal{L}_{E_xE_x}\left[-\frac{1}{T}\vec{\nabla}_x(\mu - eV)\right] + \mathcal{L}_{E_xT_x}\left[\vec{\nabla}_x\frac{1}{T}\right] \tag{B2}$$

$$\vec{j}_{T_x} = \mathcal{L}_{T_xE_x}\left[-\frac{1}{T}\vec{\nabla}_x(\mu - eV)\right] + \mathcal{L}_{T_xT_x}\left[\vec{\nabla}_x\frac{1}{T}\right] \tag{B3}$$

where μ is the chemical potential, e is the electrical charge, and V is the electrical potential. These equations, identical to the ones chosen in Ref. [19], ease the comparison of our data with the results of this reference. Besides, they enable, in the absence of vertex corrections, the computation of the relevant response functions through the general susceptibilities

$$\chi''_\nu(\omega) = \pi T\sum_\sigma \int \mathrm{d}\varepsilon \int \mathrm{d}\omega'\, \mathcal{T}(\varepsilon)\,\mathcal{A}(\varepsilon,\omega')\,\mathcal{A}(\varepsilon,\omega'+\omega) \times [f(\omega') - f(\omega'+\omega)]\left(\omega' + \frac{\omega}{2}\right)^\nu, \tag{B4}$$

with $\nu = 0,\, 1,\, 2 \equiv E_xE_x,\, E_xT_x,\, T_xT_x$, respectively. This choice of convention leads to

$$\sigma = \frac{e^2}{T}\,\mathcal{L}_{E_xE_x}\,, \tag{B5}$$

$$S = -\frac{1}{eT}\,\frac{\mathcal{L}_{E_xT_x}}{\mathcal{L}_{E_xE_x}}\,, \tag{B6}$$

$$\kappa = \frac{1}{T^2}\left[\mathcal{L}_{T_xT_x} - \frac{\mathcal{L}^2_{E_xT_x}}{\mathcal{L}_{E_xE_x}}\right], \tag{B7}$$

for the electrical conductivity σ, the Seebeck coefficient S and the thermal conductivity κ.

Appendix C: Origins of the Low-Temperature Approximation for $\mathcal{L}_{\gamma\delta}$.

To avoid analytic continuation all together, it has been proposed [31] to use $\mathcal{L}_{\gamma\delta} \simeq (\beta/\pi)^2\,\mathcal{L}_{\gamma\delta}(\tau=\beta/2)$ as an approximation for the zero frequency transport coefficients at low temperature. We have compared our results with that approximation, rewritten as:

$$\mathcal{L}_{\gamma\delta} \simeq \frac{\beta^2}{\pi^2}\int_{-\infty}^{+\infty}\mathrm{d}\omega\,\frac{\chi''_{\gamma\delta}(\vec{0},\omega)}{2\sinh\left(\frac{\beta\omega}{2}\right)}\,, \tag{C1}$$

whose derivation we give below.

Considering the right-hand term in Eq. (C1), we assume that the spectral weight of the response function is linear in frequency on the whole frequency range relevant for the integral, usually controlled at low temperature by the sinh factor. We thus have $\chi''_{\gamma\delta}(\vec{0},\omega) \simeq \omega\,\mathcal{L}_{\gamma\delta}$. Since

$$\int_{-\infty}^{+\infty}\mathrm{d}\omega\,\frac{\chi''_{\gamma\delta}(\vec{0},\omega)}{2\sinh\left(\frac{\beta\omega}{2}\right)} = \int_{-\infty}^{+\infty}\mathrm{d}\omega\,\frac{\omega}{2\sinh\left(\frac{\beta\omega}{2}\right)}\,\frac{\chi''_{\gamma\delta}(\vec{0},\omega)}{\omega}\,, \tag{C2}$$

we can approximate

$$\int_{-\infty}^{+\infty}\mathrm{d}\omega\,\frac{\chi''_{\gamma\delta}(\vec{0},\omega)}{2\sinh\left(\frac{\beta\omega}{2}\right)} \simeq \frac{2\mathcal{L}_{\gamma\delta}}{\beta^2}\int_{-\infty}^{+\infty}\mathrm{d}x\,\frac{x}{\sinh(x)}\,. \tag{C3}$$

Finally, the value of the integral

$$\int_{-\infty}^{+\infty}\mathrm{d}x\,\frac{x}{\sinh(x)} = \frac{\pi^2}{2} \tag{C4}$$

gives the expected result Eq. (C1). When the convergence of the integral is controlled by the susceptibility instead of the sinh factor, as in the renormalized classical regime, a different expression has to be devised.

Appendix D: Analytically Continued Spectral Weights of the Relevant Susceptibilities.

Let us first recapitulate our procedure for analytic continuation before we present additional results. In the case of the Seebeck response, the MaxEntAux method consists in the use of the auxiliary susceptibility

$$\chi^{aux}_\lambda(i\omega_n) = \chi_{E_xE_x}(i\omega_n) + \lambda^2\chi_{T_xT_x}(i\omega_n) + 2\lambda\,\chi_{E_xT_x}(i\omega_n) \tag{D1}$$

to enable the maximum entropy analytic continuation (MEAC) of the response function

$$\chi''_{E_xT_x}(\omega) = \frac{1}{2\lambda}\left[\chi''^{\,aux}_\lambda(\omega) - \chi''_{E_xE_x}(\vec{k},\omega) - \lambda^2\chi''_{T_xT_x}(\omega)\right], \tag{D2}$$

which possibly has a non-positive spectral weight, according to the Lehmann representation

$$\chi''_{\gamma\delta}(\vec{k},\omega) = \frac{\pi}{\mathcal{Z}}\sum_{mm'}e^{-\beta H_m}\left[e^{\beta\omega}-1\right]\langle m|\hat{\mathcal{O}}_\gamma|m'\rangle\langle m'|\hat{\mathcal{O}}_\delta|m\rangle \times\delta(\omega-(H_m-H_{m'}))\,. \tag{D3}$$

Fig. 3a and Fig. 3b compare the initial real-frequency spectral weights Eq. (B4), to those obtained after direct MEACs of the Matsubara-frequency data

$$\chi_{\gamma\delta}(i\omega_n) = \int_0^\beta \mathrm{d}\tau\, e^{i\omega_n\tau}\chi_{\gamma\delta}(\tau) = \int\frac{\mathrm{d}\omega}{\pi}\,\frac{\chi''_{\gamma\delta}(\omega)}{\omega - i\omega_n}\,, \tag{D4}$$

to which we add a Gaussian relative error of 10^{-3} on each Matsubara frequency in order to mimic quantum Monte-Carlo statistical error. For the thermoelectric response, the MaxEntAux method Eq. (D2) for $\lambda = 1$ at $U = 14$, $T = 1/10$ and for $\lambda = 0.3$ at $T = 1$, respectively, is used. The MaxEntAux method proves very efficient at capturing the qualitative features and even most of the quantitative features of the initial response functions. In particular, $\chi''_{E_xT_x}(\omega)$ has a region of negative spectral weight that is remarkably well reproduced by our approach.

As for Fig. 4a and Fig. 4b, they compare the auxiliary and thermoelectric spectral weights obtained for different values of λ from Eq. (D2). They demonstrate the overall robustness of the MaxEntAux method applied for different values of λ since most of finite-frequency features remain well preserved. The method becomes noisier at high temperature since MEACs are more difficult in that regime. Therefore, the averaging over λ-dependent results can be very useful in that case.

Appendix E: More tests on the Real-frequency and Zero-frequency Onsager Coefficients.

The MaxEntAux method also allows to extract the frequency-dependent Onsager coefficient usually unobtainable by MEAC

$$\mathcal{L}_{E_xT_x}(\omega) = \frac{1}{2\lambda}\left[\mathcal{L}^{aux}_\lambda(\omega) - \mathcal{L}_{E_xE_x}(\omega) - \lambda^2\mathcal{L}_{T_xT_x}(\omega)\right] \tag{E1}$$

by using the auxiliary functions as in Eq. (D2). Fig. 5a and Fig. 5b compare the initial real-frequency Onsager coefficients Eq. (B4), at $U = 14$, to those obtained with

Eq. (E1) above and direct MEACs of the Matsubara-frequency data, with an added relative noise of 10^{-3}. The analytic expression Eq. (B1) that relates those coefficients to the zero-frequency limit of susceptibilities has also been used.

In MaxEntAux method Eq. (E1), we take $\lambda = 1$ at $T = 1/10$ and $\lambda = 0.3$ at $T = 1$, respectively. Although the latter case is already presented in the main text, it is repeated to allow an easier comparison with the lower temperature data. Once again, the MaxEntAux method proves very efficient at capturing the qualitative features, and even most of the quantitative features, of the initial frequency-dependent Onsager coefficients. However, the MEACs tend to slightly oscillate around the initial Onsager coefficients obtained from Eq. (B4) since the almost imperceptible oscillations of the analytically continued spectral weights are amplified by the division by ω necessary to obtain the Onsager coefficients in Eq. (B1). The dotted lines of Fig. 5b shows the exact diagonalization results of Ref. [19], which compare well with our results. The differences between exact diagonalization (ED) and the combination of continuous-time quantum Monte Carlo (CTQMC) and MEAC explain that the comparison is not perfect. Indeed, ED usually finds more numerous and sharper structures than in reality because of its finite bath, whereas CTQMC+MEAC tends to smooth them out.

As for Fig. 6a and Fig. 6b, they compare the auxiliary and thermoelectric frequency-dependent Onsager coefficients obtained for different values of λ from Eq. (D2). In the same way as above for the relevant susceptibilities, they demonstrate the overall robustness of the MaxEntAux method applied for different values of λ.

Fig. 7a and Fig. 7b compare only the zero-frequency values of the aforementioned frequency-dependent Onsager coefficients, $\mathcal{L}_{\gamma\delta}$, obtained before and after the MEAC, for $T = 1/10$ and $T = 1$, ($U = 14$) respectively. In addition to the comparison of our results with those of Ref. [19] for $T = 1$, a comparison with the low-temperature approximation, Eq. (C1), is also shown for both temperatures. The comparison with the results of Ref. [19] obtained directly in real-frequency with an ED solver is reasonable, but this comparison does not check only the validity of MaxEntAux since a different solver has been used. While the results obtained with the approximation Eq. (C1) improve as the temperature decreases, the MaxEntAux method is still competitive. Eq. (C1) would not be valid if the system was in the renormalized-classical regime. For finite-frequency transport quantities, there is no approximation that replaces Eq. (C1) to avoid direct analytic continuation. The MaxEntAux method seems to be a robust and accurate method for the extraction of the relevant transport coefficients.

Appendix F: Benchmarks for lower temperature transport coefficients.

Fig. 8a and Fig. 8b show the electrical conductivity σ Eq. (B5), the Seebeck coefficient S Eq. (B6) and the thermal conductivity κ Eq. (B7) at $T = 1/10$ and at $T = 1$, respectively, for $U = 14$. Once again, the MaxEntAux method proves more accurate than the other methods, except for the thermal conductivity at $T = 1/10$ where the low-temperature approximation Eq. (C1) is better. We explain this discrepancy by the sensitivity of Eq. (B7) for κ to the smallest of errors on the value of the Onsager coefficient $\mathcal{L}_{T_xT_x}$. Indeed, we saw in Fig. 7a that it was slightly off. Limitations of the low temperature approximation Eq. (C1) are discussed at the end of the previous section.

Appendix G: Convergence of Matsubara frequency sums: New expressions for the uniform susceptibilities $\chi_{E_xT_x}(i\omega_n)$ and $\chi_{T_xT_x}(i\omega_n)$ without vertex corrections.

The calculation of Matsubara-frequency susceptibilities, that are input to the MaxEntAux method, is difficult by itself. In particular, the expressions given in Ref. [41] for the thermoelectric and thermal conductivity transport coefficients lack the terms that make the summations over Matsubara frequencies (ip_m below) convergent. The Master's thesis of A.-M. Gagnon Ref. [28] gives us new convergent expressions for the bubble contribution to $\chi_{E_xT_x}(i\omega_n)$ and $\chi_{T_xT_x}(i\omega_n)$. Convergence of the terms containing vertex corrections should be easier to obtain. They are not discussed here. Her results are summarized here:

$$\chi_{E_xE_x}(i\omega_n) = -\frac{e^2}{\beta}\sum_{\vec{k},\sigma}\left(\frac{\partial\varepsilon_{\vec{k}}}{\partial k_x}\right)^2\sum_{ip_m}\mathcal{G}_\sigma(\vec{k},ip_m)\mathcal{G}_\sigma(\vec{k},ip_m+i\omega_n)\,, \tag{G1}$$

$$\chi_{E_xT_x}(i\omega_n) = -\frac{e}{\beta}\sum_{\vec{k},\sigma}\left(\frac{\partial\varepsilon_{\vec{k}}}{\partial k_x}\right)^2\sum_{ip_m}\left[\left(ip_m+\frac{i\omega_n}{2}\right)\mathcal{G}_\sigma(\vec{k},ip_m)\mathcal{G}_\sigma(\vec{k},ip_m+i\omega_n)-\mathcal{G}_\sigma(\vec{k},ip_m)\right], \tag{G2}$$

$$\begin{aligned}\chi_{T_xT_x}(i\omega_n) = -\frac{1}{4\beta}\sum_{\vec{k},\sigma}\left(\frac{\partial\varepsilon_{\vec{k}}}{\partial k_x}\right)^2\sum_{ip_m}\Big[&-(\langle\omega\rangle_\sigma(\vec{k})-ip_m)\mathcal{G}_\sigma(\vec{k},ip_m+i\omega_n)+2-(\langle\omega\rangle_\sigma(\vec{k})-ip_m-i\omega_n)\mathcal{G}_\sigma(\vec{k},ip_m)\\ &-2(2ip_m+i\omega_n)\Big(\mathcal{G}_\sigma(\vec{k},ip_m+i\omega_n)+\mathcal{G}_\sigma(\vec{k},ip_m)\Big)+(2ip_m+i\omega_n)^2\mathcal{G}_\sigma(\vec{k},ip_m)\mathcal{G}_\sigma(\vec{k},ip_m+i\omega_n)\Big]\,,\end{aligned} \tag{G3}$$

where, in the case of the Hubbard model,

$$\langle\omega\rangle_\sigma(\vec{k}) = \int \omega\, \mathcal{A}(\vec{k},\omega)\, \mathrm{d}\omega = \varepsilon_{\vec{k}} - \mu + U n_\sigma\,. \tag{G4}$$

n_σ represents the filling of electrons with spin σ.

Although the above sums are convergent, for large $i\omega_n$ one needs to be careful. Convergence can be accelerated greatly by using some of the algorithms that appear in section C of appendix C of Ref. [40].

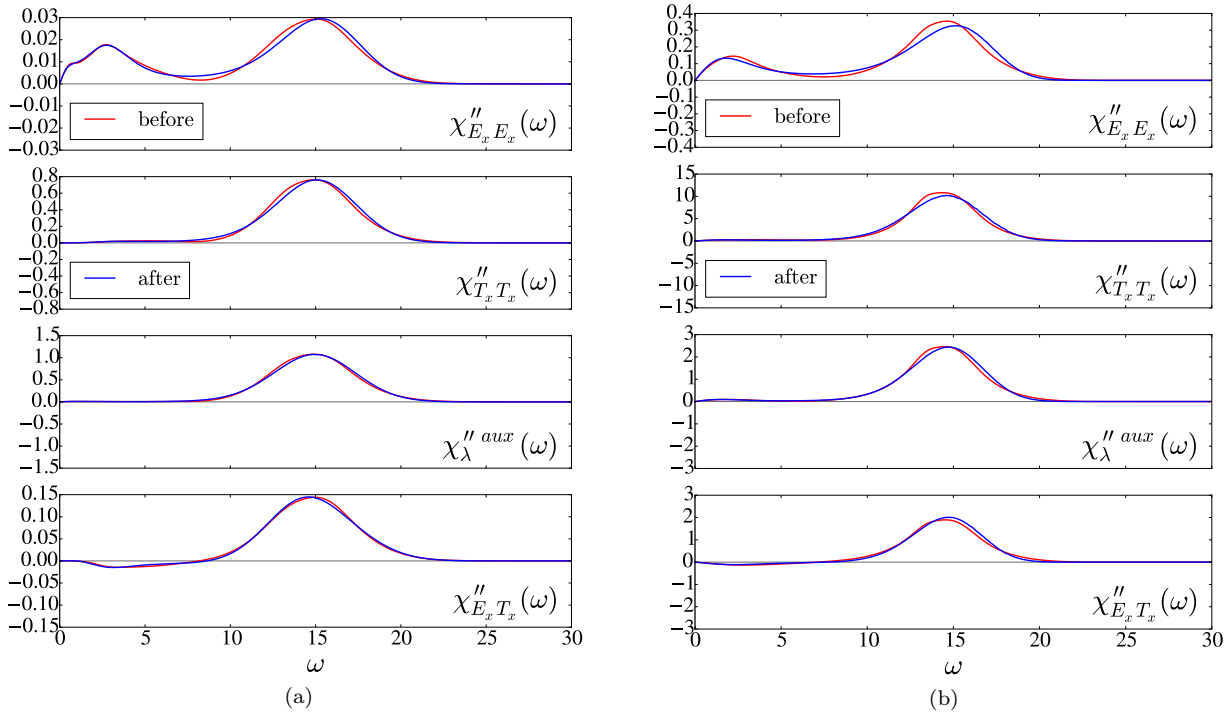

Figure 3. Comparison between the initial real-frequency response functions' spectral weights (in red) and the ones obtained after direct MEACs of the Matsubara-frequency data and the MaxEntAux method (in blue) Eq. (D2). (a) Results for $\lambda = 1$ at $T = 1/10$. (b) Results for $\lambda = 0.3$ at $T = 1$.

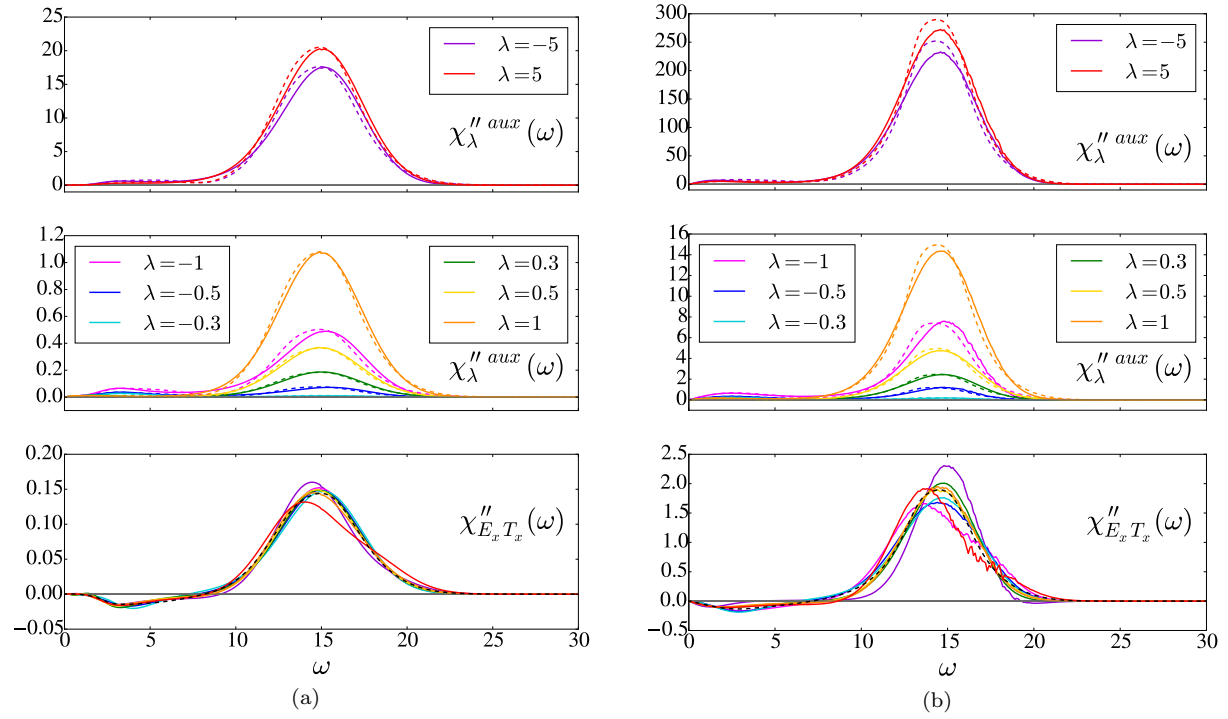

Figure 4. Comparison of the auxiliary and thermoelectric spectral weights obtained for different values of λ from Eq. (D2). The results before (dashed lines) and after (solid lines) the MEACs and the MaxEntAux method are shown. The black dashed lines in the lowest panels represent the expected thermoelectric spectral weight obtained from Eq. (B4). (a) Results at $T = 1/10$. (b) Results at $T = 1$.

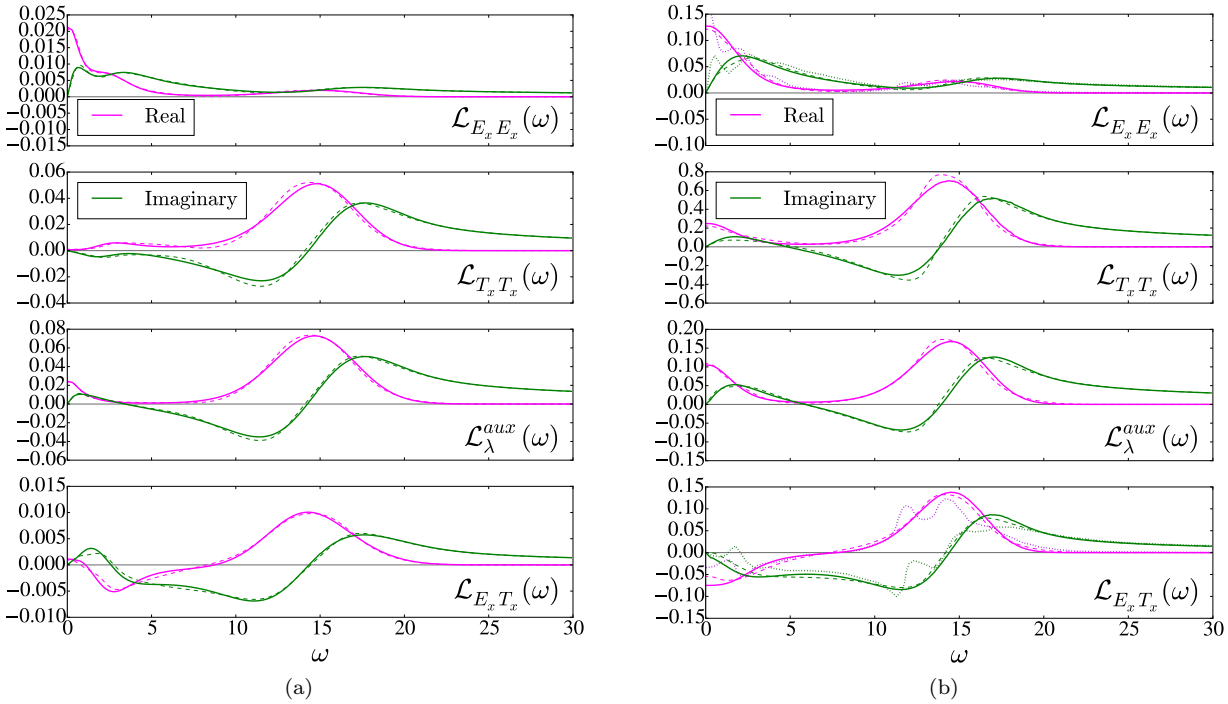

Figure 5. Comparison between the initial real-frequency Onsager coefficients extracted from the analytic expression Eq. (B4) using Eq. (B1) (dashed lines) to those obtained after direct MEACs of the Matsubara-frequency data and the MaxEntAux method Eq. (E1) (solid lines). (a) Results for $\lambda = 1$ at $T = 1/10$. (b) Results for $\lambda = 0.3$ at $T = 1$. The dotted lines show the results of Ref. [19] at $T = 1$ for comparison.

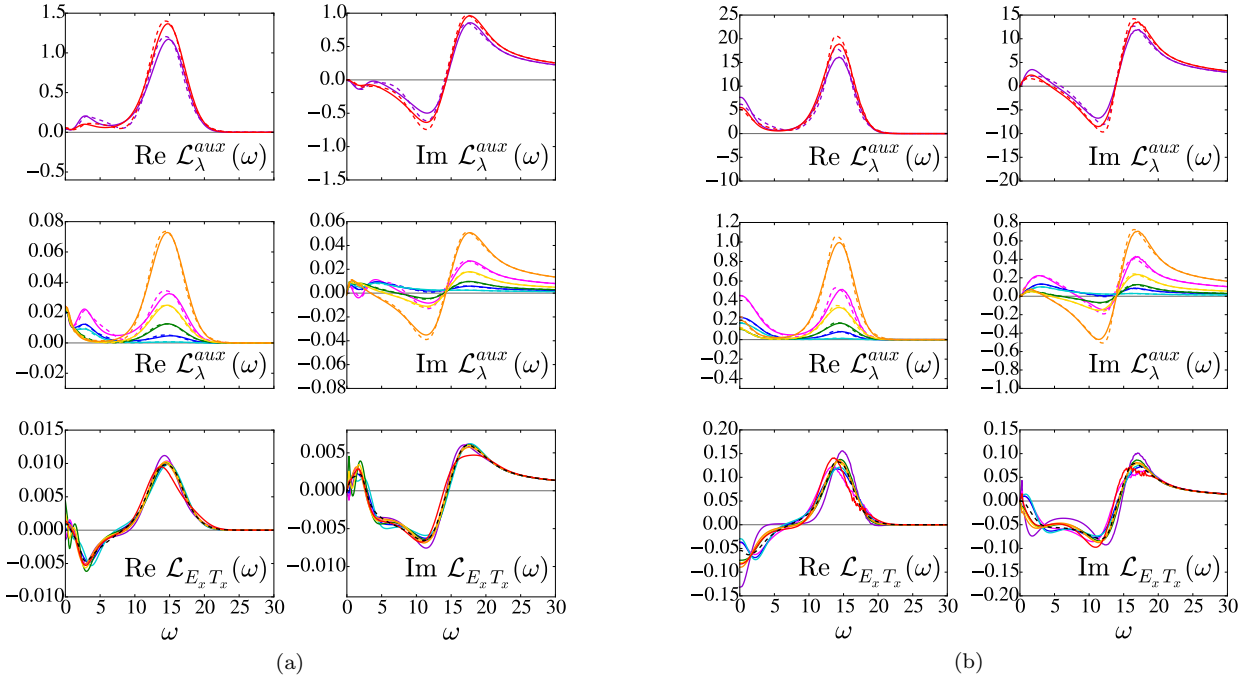

Figure 6. Comparison of the auxiliary and thermoelectric frequency-dependent Onsager coefficients obtained for different values of λ from Eq. (E1). The results before (dashed lines) and after (solid lines) the MEACs and the MaxEntAux method are shown. The color code is the same as the one of Fig. 4. The black dashed lines in the lowest panels represent the expected thermoelectric frequency-dependent Onsager coefficient obtained from Eq. (B4) using Eq. (B1). (a) Results at $T = 1/10$. (b) Results at $T = 1$.

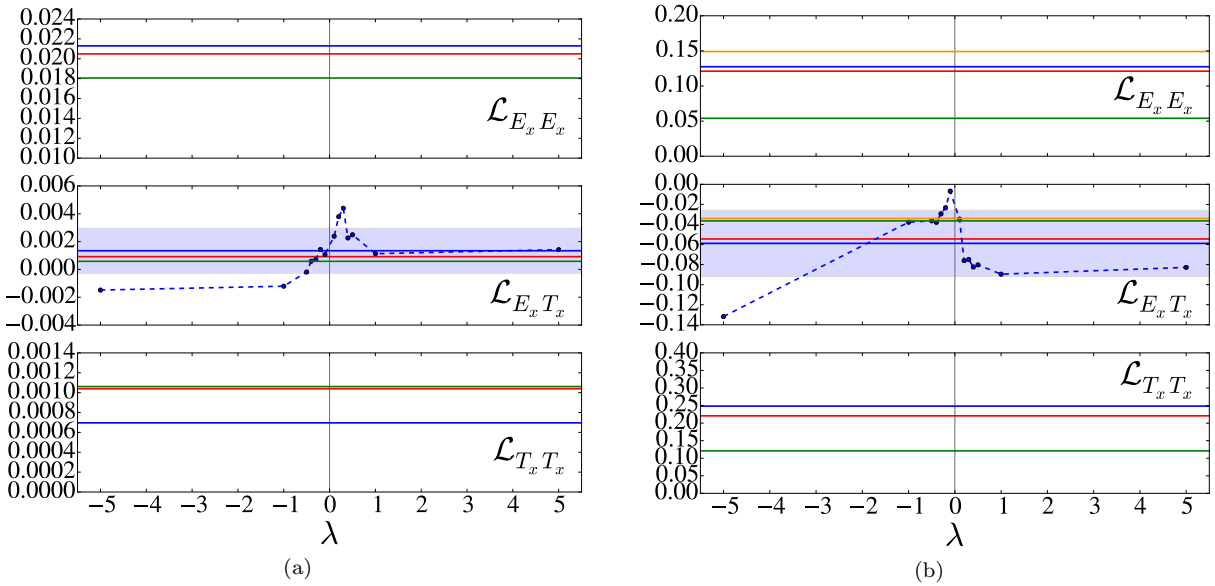

Figure 7. Zero-frequency values of the frequency-dependent Onsager coefficients shown in Fig. 5. The comparison is made between the results before (red solid lines) and after (blue dashed lines) the MEACs and the MaxEntAux method for different values of λ. The blue solid lines and blue area represent the mean value and the error span of the λ-dependent Onsager coefficient $\mathcal{L}_{E_x T_x}$ (blue points), respectively. The green lines show the results of the low-temperature approximation Eq. (C1). (a) Results at $T = 1/10$. (b) Results at $T = 1$. The orange lines show the results of Ref. [19] at $T = 1$ for comparison.

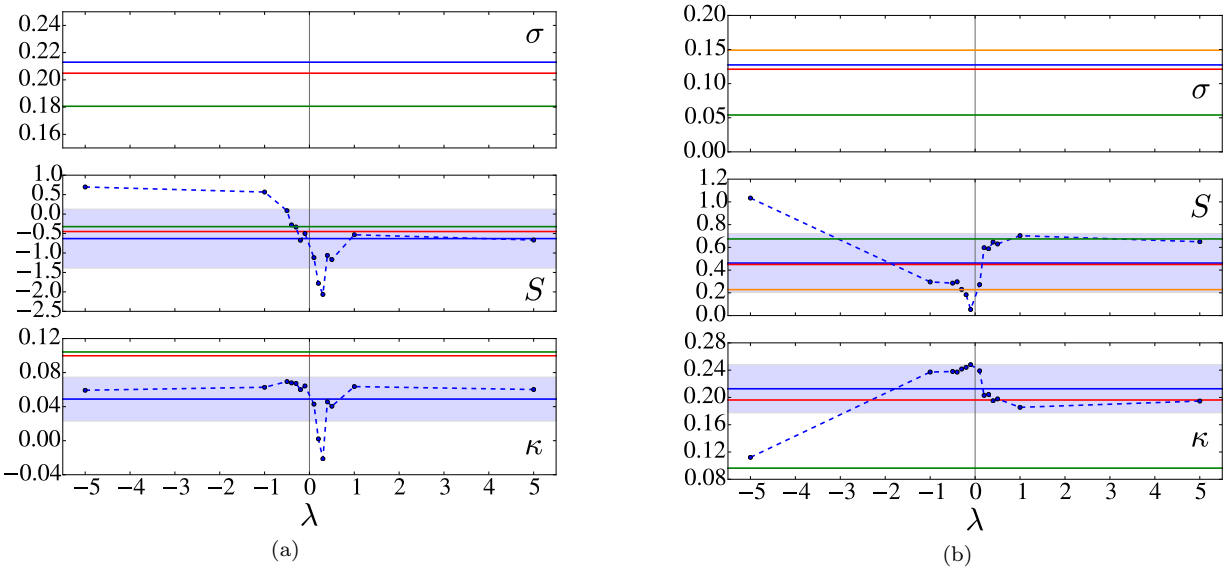

Figure 8. Electrical conductivity, Seebeck coefficient, and thermal conductivity extracted from Eq. (B5) and Eq. (B6), and Eq. (B7), respectively. The comparison is made between the results before (red solid lines) and after (blue dashed lines) the MEACs and the MaxEntAux method for different values of λ. The blue solid lines and blue area represent the mean value and the error span of the λ-dependent results (blue points), respectively. The green lines show the results of the low-temperature approximation Eq. (C1). (a) Results at $T = 1/10$. (b) Results at $T = 1$. The orange lines show the results of Ref. [19] at $T = 1$ for comparison.